ACSNANO
www.acsnano.org
ARTICLE

Ultrasensitive Characterization of Mechanical Oscillations and Plasmon Energy Shift in Gold Nanorods

Giancarlo Soavi,[*,†,¶] Iacopo Tempra,[†] Maria F. Pantano,[‡] Andrea Cattoni,[§] Stéphane Collin,[§] Paolo Biagioni,[†] Nicola M. Pugno,[‡,∥,⊥] and Giulio Cerullo[*,†,#]

[†]Department of Physics, Politecnico di Milano, P.zza L. Da Vinci 32, 20133 Milano, Italy

[‡]Laboratory of Bio-inspired & Graphene Nanomechanics, Department of Civil, Environmental and Mechanical Engineering, Università di Trento, via Mesiano 77, 38123 Trento, Italy

[§]Laboratoire de Photonique et de Nanostructures, CNRS, Université Paris-Saclay, route de Nozay, F-91460 Marcoussis, France

[∥]Center for Materials and Microsystems, Fondazione Bruno Kessler, Via Sommarive 18, 38123 Povo (TN), Italy

[⊥]School of Engineering and Materials Science, Queen Mary University of London, Mile End Road, London E1 4NS, United Kingdom

[#]IFN-CNR, P.zza L. Da Vinci 32, 20133 Milano, Italy

Supporting Information

ABSTRACT: **Mechanical vibrational resonances in metal nanoparticles are intensively studied because they provide insight into nanoscale elasticity and for their potential application to ultrasensitive mass detection. In this paper, we use broadband femtosecond pump−probe spectroscopy to study the longitudinal acoustic phonons of arrays of gold nanorods with different aspect ratios, fabricated by electron beam lithography with very high size uniformity. We follow in real time the impulsively excited extensional oscillations of the nanorods by measuring the transient shift of the localized surface plasmon band. Broadband and high-sensitivity detection of the time-dependent extinction spectra enables one to develop a model that quantitatively describes the periodic variation of the plasmon extinction coefficient starting from the steady-state spectrum with only one additional free parameter. This model allows us to retrieve the time-dependent elongation of the nanorods with an ultrahigh sensitivity and to measure oscillation amplitudes of just a few picometers and plasmon energy shifts on the order of 10^{-2} meV.**

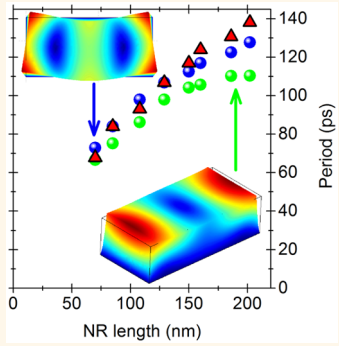

KEYWORDS: *ultrafast spectroscopy, coherent oscillations, metal nanoparticles*

The study of the relaxation mechanisms of optically excited metal nanoparticles (NPs) on the ultrafast time scale is of fundamental importance for the understanding of their electronic and mechanical properties. In these systems, light−matter interaction is dominated by localized surface plasmons (LSPs), that is, the collective oscillations of the free electrons in the metal, which are responsible for a substantial extinction of the incident light by either absorption or scattering. Since LSP resonances are extremely sensitive to the environment and strongly depend on the NP material, size, and shape,[1] metal NPs are ideal candidates for biosensing applications.[2,3] Moreover, metal NPs behave as nanomechanical oscillators with extremely high frequencies, in the range of tens to hundreds of GHz, and many efforts have been devoted to the detection of their vibrational modes, either in the frequency domain[4] or in the time domain.[5−15] On the one hand, these vibrations provide access to the elastic properties of the metal at the nanoscale and their dependence on the internal structure of the NP;[10] on the other hand, such mechanical nanoresonators can be used as ultrasensitive sensors and mass detectors.[16−18] Time domain detection of vibrational modes in metal NPs is typically performed in a pump−probe configuration. Following photoexcitation by a femtosecond pump pulse and ultrafast LSP dephasing,[19] the conduction-band population of the metal NP is excited into a nonthermal electronic distribution which relaxes, on the hundred femtosecond time scale,[20,21] into a thermalized electronic distribution *via* electron−electron interaction (EEI). The hot electron gas equilibrates with the cold lattice on the picosecond time scale *via* electron−phonon interaction (EPI), and finally, the lattice cools on the nanosecond time scale *via* energy transfer to the environment, that is, phonon−phonon interaction (PPI), which brings back

Received: November 2, 2015
Accepted: January 14, 2016
Published: January 14, 2016

DOI: 10.1021/acsnano.5b06904
ACS Nano 2016, 10, 2251−2258

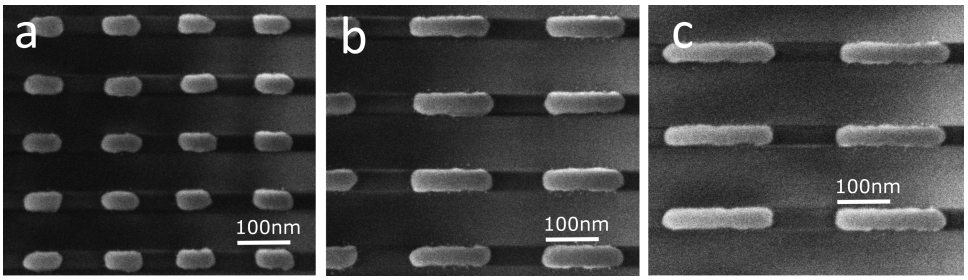

Figure 1. SEM images of three different arrays of gold NRs with lengths of (a) 70 nm, (b) 150 nm, and (c) 200 nm.

the metal NP to the thermal equilibrium. If the time scale of lattice heating *via* EPI is much shorter than the characteristic period(s) of the NP vibrational mode(s), coherent oscillations are impulsively launched in the NP.[22] As the NP vibrates, the periodic changes in its shape and/or aspect ratio modulate the spectral position of the LSP resonance and can be detected by a time-delayed probe pulse. Oscillations are characterized by their period and damping time, which depend on the bulk properties of the material, size, and shape of the NP and its interaction with the environment. In particular, the period of the oscillations provides information on the geometrical (size and shape) properties, the nanocrystallinity, the speed of sound, and the Young modulus of the sample;[12,23] the damping time can be used as a probe of the NP interaction with the environment, especially for experiments on isolated metal NPs,[13,14] where the effect of inhomogeneous broadening is suppressed.

Despite this wealth of information, the accurate characterization of the amplitude and wavelength dependence of the NP oscillations remains challenging. These parameters are crucial as they intrinsically account for the mechanical properties of the NP and they directly relate to the LSP peak shift, which is the best fingerprint to be used for sensing applications. Clearly, an ideal sensor must be able to detect the smallest possible peak shift, which corresponds to the highest sensitivity to the geometrical (size and shape) changes of the oscillating NP. Recently, direct imaging of the time-dependent atomic-scale deformation of NPs has been achieved by means of time-resolved X-ray or electron diffraction,[24−26] both of which are very demanding techniques and, due to their current sensitivity limits, can only probe relatively large amplitude oscillations. In this work, we apply broadband femtosecond pump−probe spectroscopy to quantitatively study the extensional mechanical oscillations of macroscopic arrays of gold nanorods (NRs) with different aspect ratios, fabricated by electron beam lithography (EBL), and with high size uniformity. We follow in real time the mechanical elongation of the NRs by measuring the transient shift of the LSP band. Due to the capability of broadband and high-sensitivity detection of the time-dependent LSP resonance, we are able to develop a simple model that accurately describes the transient variation of the LSP extinction spectrum starting from its steady-state description, with only one additional free parameter. This allows us to estimate the time-dependent elongation of the NRs with ultrahigh sensitivity and measure oscillations in a truly perturbative regime, with amplitudes down to just a few picometers.

RESULTS AND DISCUSSION

Linear Absorption Spectra. Eight arrays of gold NRs with different lengths were fabricated on glass substrates by EBL (see Methods for details). The height and width of the NRs were kept constant at $h \approx 20$ nm and $w \approx 30$ nm, respectively, while their length L was varied from 70 to 200 nm, resulting in a large tunability of the LSP resonance peak from about 1.9 eV (for the 70 nm rod) to about 1.1 eV (for the 200 nm rod). Figure 1 shows scanning electron microscope (SEM) images for three representative samples. Each array was fabricated over a quite large area of 1 mm^2. The excellent uniformity of size and shape of the NRs and their perfect alignment minimize inhomogeneous broadening effects and allow for their far-field characterization without the use of more demanding single-particle spectroscopies.[13−15]

Figure 2a shows as solid lines the measured extinction spectra of the eight arrays, with light linearly polarized parallel

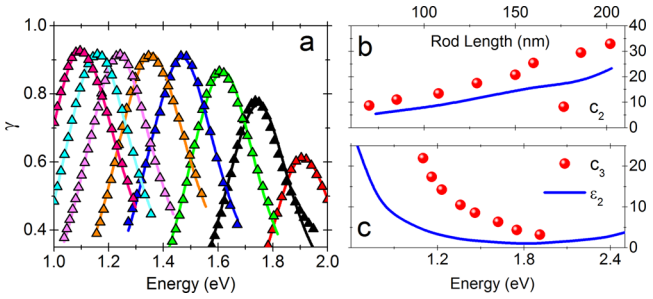

Figure 2. (a) Measured (solid line) and fitted (symbols) extinction factor γ for the eight arrays of gold NRs, with lengths ranging from 70 to 200 nm. The fit is performed according to the Gans theory for isolated NRs (ref 28), as described in the text. (b) Theoretical (solid line, assuming oblate spheroids) and fitted (symbols) depolarization factor along the main axis of the gold NRs as a function of the rod length. (c) Experimental (solid line) imaginary part of the dielectric constant of gold from ref 29 and additional broadening (symbols) obtained from the fitting described in the text (eq 1).

to the long NR axis, which shows the expected red shift of the LSP resonance with increasing length. A good fit to the extinction of a NR ensemble in the dipole approximation can be obtained by the Gans theory, which is an extension of Mie theory to prolate and oblate spheroidal NPs.[27,28] In this framework, the extinction coefficient for an ensemble of isolated (*i.e.*, noninteracting) NRs can be expressed as

$$\gamma(\omega, c_1, c_2, c_3) = c_1 \epsilon_m^{3/2} \frac{\epsilon_2(\omega)}{(\epsilon_1(\omega) + c_2\epsilon_m)^2 + \epsilon_2(\omega)^2 + c_3^2} \cdot \hbar\omega \quad (1)$$

where $\hbar\omega$ is the photon energy, ϵ_m is the average dielectric constant of the surrounding medium, $\epsilon_1(\omega)$ and $\epsilon_2(\omega)$ are the real and imaginary parts of the gold dielectric constant, and c_1,

DOI: 10.1021/acsnano.5b06904
ACS Nano 2016, 10, 2251−2258

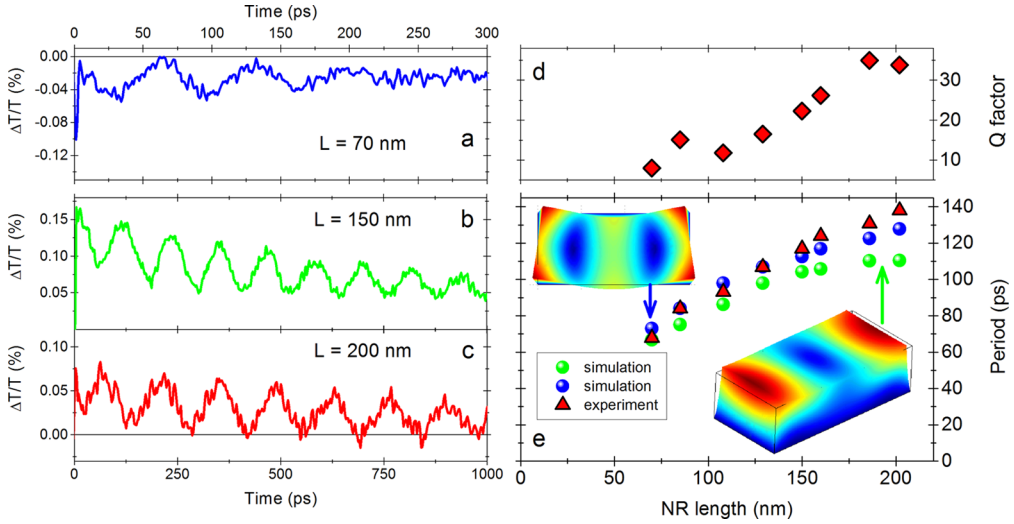

Figure 3. $\Delta T/T$ dynamics for three NRs with different length, L: (a) L = 70 nm, recorded at 1.8 eV probe photon energy; (b) L = 150 nm, recorded at 1.3 eV probe photon energy; (c) L = 200 nm, recorded at 1.05 eV probe photon energy. Quality factor (d) and period (e) of the extensional coherent oscillations as a function of the NR length together with numerical simulations and sketch of two possible vibrational modes.

c_2, and c_3 are fitting parameters, which are constant for a given NR geometry. Since we are dealing with aligned NRs excited with light polarized along the longitudinal axis, eq 1 has been simplified accordingly (*i.e.*, neglecting extinction of light polarized along the transverse direction) with respect to ref 28. The results of the fit, reported in Figure 2a as triangles, are in excellent agreement with the experimental extinction spectra. In particular, we used ϵ_m = 1.56 as the average dielectric constant of the surrounding medium (air and glass), while $\epsilon_1(\omega)$ and $\epsilon_2(\omega)$ were taken from the experimental values of ref 29. Concerning the fitting parameters, c_1 is a scale factor, accounting for the overall illumination and detection efficiencies, and for the number of particles within the focal volume, c_2 is a function of the depolarization factor for the longitudinal LSP resonance defined according to ref 28 (for simplicity, in the following, we will refer to c_2 directly as the depolarization factor), and c_3 is an additional broadening term. Let us now focus our attention on the latter two terms. The depolarization factor c_2 depends on the geometrical parameters of the NR and determines the peak position of the LSP resonance. Within the dipolar approximation, c_2 can be easily calculated analytically only for prolate or oblate spheroids in a homogeneous environment. Since these geometrical shapes and conditions do not accurately describe our samples, we chose to keep c_2 as a fitting parameter, thus providing a geometrical degree of freedom to match the theory with the experiments. Figure 2b compares the c_2 values extracted from our fit with the theoretical values calculated for an ideal prolate spheroid, according to ref 28. The behavior of the two parameters is qualitatively the same, with most of the deviations occurring, as expected, for the longer NRs (*i.e.*, lower resonant energies), for which the geometrical difference with respect to a spheroid becomes more pronounced. Finally, c_3 is an additional broadening term that accounts for radiative damping and uncertainties in the experimental dielectric constant, together with possible residual inhomogeneous broadening. Figure 2c compares the values of c_3 extracted from the fits with the imaginary part ϵ_2 of the gold dielectric constant from ref 29. The largest contribution is observed for longer NRs and can be tentatively attributed to the larger radiative damping for more elongated particles. In summary, the simple analytical model expressed by eq 1 enables an excellent fit of the extinction spectra of all NR samples, and it will be used in the following to describe their transient variations due to the impulsively excited mechanical vibrations.

Pump−Probe on Gold NRs and Mechanical Simulations. We performed ultrafast pump−probe experiments on all eight arrays of gold NRs, which were excited at 1.6 eV by a 100 fs pulse and probed over a broad spectral range in the visible and near-IR by a white-light continuum (WLC; see Methods for details of the experimental setup). Pump and probe polarizations were parallel and aligned with the long axis of the NRs. For each sample, we recorded a two-dimensional (2D) map of the differential transmission ($\Delta T/T$) as a function of the probe photon energy and the pump−probe delay. In this study, we are not interested in the energy relaxation processes due to EEI, EPI, and PPI, so we subtract from the $\Delta T/T$ data the dynamics that reflect these processes (corresponding to exponential decays) until we are left with the oscillatory signals associated with the impulsively excited mechanical vibrations of the NRs. In pump−probe spectroscopy, optical signatures of the mechanical oscillations are observed only for those modes that significantly modify the aspect ratio of the NRs and thus shift their LSP resonance. There are mainly two families of vibrational modes that induce variations of the aspect ratio: the radial breathing modes and the longitudinal (*i.e.*, extensional) modes, both of which can be analytically modeled for NRs in vacuum under the assumption that the NR length largely exceeds the radius.[23] Figure 3a shows a $\Delta T/T$ time trace for the L = 70 nm NR, recorded at 1.8 eV probe photon energy. We clearly recognize a coherent oscillation, which based on the simulations described below we assign to the extensional mode of the NRs, with a damped amplitude due to energy transfer from the lattice to the environment. The oscillation period increases for increasing rod length, as demonstrated in Figure 3b,c, reporting results for NR ensembles with L = 150 nm and L = 200 nm, respectively. The oscillation period of these extensional modes as a function of the NR length is shown in Figure 3e.

DOI: 10.1021/acsnano.5b06904
ACS Nano 2016, 10, 2251−2258

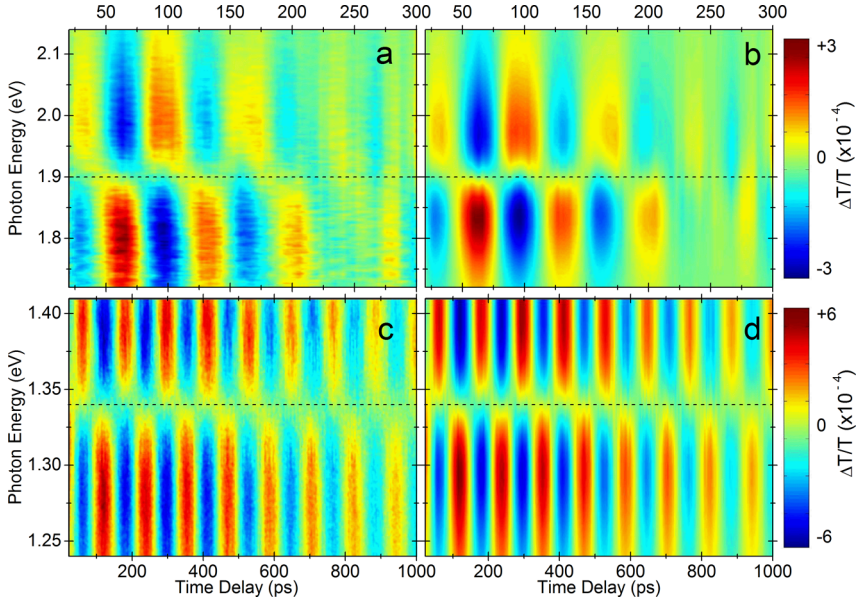

Figure 4. (a,c) Two-dimensional $\Delta T/T$ maps of the coherent oscillations as a function of probe photon energy and pump−probe delay in two arrays of gold NRs with lengths of 70 and 150 nm, respectively. (b,d) Fits obtained according to the model described in the text. The dotted lines correspond to the LSPs extinction peak (from Figure 2).

In order to gain further insights into the nature of the mechanical oscillations of the gold NRs, we performed an eigenvalue analysis with the COMSOL Multiphysics software (see Methods for details) for five possible oscillation geometries given the boundary conditions of our experiment (*i.e.*, constraints at the gold/glass substrate). Among these, only two could correctly reproduce the experimentally observed dependence of the oscillation period on the NRs length, with a maximum discrepancy of less than 20%, in correspondence to the longest (200 nm) NR. This error is likely due to a slightly different geometry of the simulated NRs (edge shape) with respect to the real ones. Although all five different modes obtained by eigenvalue analysis have a similar oscillation period, the choice of the selected mechanical oscillations was possible due to the experimental availability of a large range of NR aspect ratios. In fact, given a single NR geometry, the choice among different possible vibrational modes simply based on the values of the oscillation period obtained from FE simulations could be misleading, while tracing the period VS nanorod length dependence allows a straightforward assignment (see Supporting Information for details). It is worthy to note that although both the selected simulated oscillations might contribute to the observed signal, one of them (green circles in Figure 3e) seems to have a stronger influence on the NR aspect ratio, and thus we expect it to affect the LSP peak shift more significantly.[30]

We also observe that the quality factor of the extensional mode, defined as $\pi(\tau_{period}/\tau_{damping})$ (Figure 3d), increases with the NR length. Such a relationship might also be influenced by the presence of a significant interfacial dissipation[31] between the NR and the substrate and is qualitatively similar to that found for a III−V nanopillar integrated with a silicon photonic crystal cavity.[32]

Modeling of the Differential Transmission Spectra. While a time trace at a single probe photon energy, as shown in Figure 3, is sufficient to extract the period and damping time of the extensional coherent oscillations of the NRs, the availability of broadband $\Delta T/T$ maps across the LSP resonance is of crucial importance to enable accurate modeling of the amplitude of the nanomechanical oscillations. Figure 4 shows the 2D maps of the oscillatory component of the $\Delta T/T$ signal for two set of NRs with lengths of L = 70 nm (panel a) and L = 150 nm (panel c). For these two samples, the WLC spectrum covers the entire LSP bandwidth. This oscillatory pattern is consistent with a periodic red and blue shift of the NR extinction spectrum, with a minimum at the peak of the LSP resonance and a π phase shift between oscillations on the two sides of the LSP peak. We fit the $\Delta T/T$ transient spectra, as a function of the probe photon energy $\hbar\omega$ and pump−probe delay τ, as

$$\frac{\Delta T}{T}(\omega, \tau) = \frac{T^*(\omega, \tau) - T(\omega)}{T(\omega)} \quad (2)$$

where $T(\omega) = 1 - \gamma(\omega, c_1, c_2, c_3)$ is the unperturbed transmission, obtained from the fit of the linear extinction coefficient by eq 1. $T^*(\omega, \tau)$ is the transmission of the NRs perturbed by the pump pulse, which we write as

$$T^*(\omega, \tau) = 1 - \gamma^*(\omega, c_1, c_2 + \Delta c_2(\tau), c_3) \quad (3)$$

where c_1 and c_3 are fixed to the values extracted from the fit of the linear extinction coefficient and only c_2 is varied. We are thus able to precisely reproduce our experimental data (Figure 4b,d) by using *only one time-dependent fitting parameter* $\Delta c_2(\tau)$, which describes the variations of the aspect ratio of the NR, and thus of the depolarization factor of the LSP resonance. This model clarifies the physical origin of the optical signatures observed for the nanomechanical oscillations, which are coupled to the $\Delta T/T$ signal due to the strong dependence of the LSP resonance peak position on the NR aspect ratio.[28] An increase (reduction) of the NR length, as in an extensional mode, leads to a red (blue) shift of the LSP resonance. This observation clearly has its counterpart in the frequency domain. Figure 5 shows the probe photon energy dependence of the Fourier transform, in amplitude and phase, of the extensional coherent oscillations for the two NRs under investigation. For

DOI: 10.1021/acsnano.5b06904
ACS Nano 2016, 10, 2251−2258

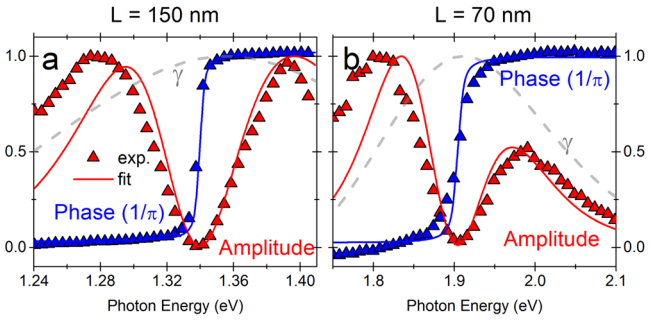

Figure 5. Fourier transform (amplitude and phase) of the extensional coherent oscillations as a function of the probe photon energy for the 150 and 70 nm gold NR arrays. Triangles, experimental data; solid lines, fits according to the model described in the text; dashed lines, extinction coefficient of the NRs.

very small energy shifts, the oscillation amplitude in the frequency domain clearly corresponds to the first derivative of the extinction spectrum, that is, of the LSP resonance. In fact, as previously discussed, the oscillations have zero amplitude, corresponding to the LSP peak and two maxima on the red and blue side (at lower and higher frequencies). Moreover, the oscillations at higher and lower frequencies with respect to the LSP peak have opposite phase. All of these features are well described by our model (solid line in Figure 5). It is interesting to compare the frequency dependence of the amplitude of the Fourier transform for the different NR lengths: we observe that it is symmetric around the LSP resonance for the 150 nm NR (panel a), while it is strongly asymmetric for the 70 nm NR (panel b), as accurately reproduced by our model. We attribute the asymmetry observed in the case of the 70 nm NR to the proximity of the LSP resonance to the interband transitions of gold (at ≈2.3 eV), which act as an additional broadening term that is naturally included in the imaginary part of the dielectric constant $\epsilon_2(\omega)$.[29]

Ultrasensitive Characterization of Mechanical Oscillations and Energy Shift. We now exploit the results of the fitting procedure to quantitatively characterize the amplitude of the mechanical oscillations of the gold NRs. From the fittings, we obtain the time-dependent variation of the depolarization factor $\Delta c_2(\tau)$, which oscillates with the same period and damping time of the extensional mode of the NR under investigation. Since the depolarization factor $c_2(L)$ is a function of the rod length (as shown in Figure 2b), the elongation of the NR can be expressed, to the first order, as

$$\Delta L(\tau) = \frac{\Delta c_2(\tau)}{\mathrm{d}c_2/\mathrm{d}L} \tag{4}$$

where $\mathrm{d}c_2/\mathrm{d}L$ is calculated as the derivative of the interpolated values of c_2 as a function of the NR length L (Figure 2b). The time-dependent NR elongations for our experimental data are shown in Figure 6a,b; we obtain a maximum elongation $\Delta L_{max} \cong 3$ (5) pm for the 70 (150) nm NR, thus indicating ultrahigh sensitivity, in the range of a few picometers, in the detection of the mechanical deformations of the NR under investigation. Besides the variation of the depolarization factor, from the fits, we can also extract the temporal evolution of the energy shift for the LSP resonance by simply tracking the spectral position of the minimum (maximum) in the perturbed transmission T^* (extinction factor γ^*). The normalized energy shift $\Delta E/E$ of the LSP peak as a function of time is also shown in Figure 6a,b and amounts to a few tens of microelectronvolts. To further support the validity of our analysis and fitting procedure, we compare the relative energy shift $\Delta E/\Delta L$ obtained from the fitting of the $\Delta T/T$ data with that obtained by electromagnetic numerical simulations with the finite-difference time domain (FDTD) method. In the simulations, we vary the aspect ratio of each NR while keeping its volume constant and calculate the energy shift of the longitudinal localized plasmon resonance as a function of the NR elongation. From the FTDT simulations, we extract (i) $\Delta E/\Delta L$ = 12 meV/nm *versus* $\Delta E/\Delta L$ = 15 meV/nm (from pump−probe) for the 70 nm NR and (ii) $\Delta E/\Delta L$ = 7 meV/nm *versus* $\Delta E/\Delta L$ = 5 meV/nm (from pump−probe) for the 150 nm NR. This very good agreement between experimental results (from pump−probe) and numerical simulations further supports the validity of our model and confirms our ability to detect NR elongations of the order of a few picometers.

Given the fluencies employed during the experiments (between 100 and 300 μJ/cm^2) and the simulated absorption cross sections of the nanoparticles (on the order of 10^3 to 10^4 nm^2 for different NR lengths), application of the two-temperature model predicts an increase in the lattice temperature between 5 and 50 K (see Supporting Information for

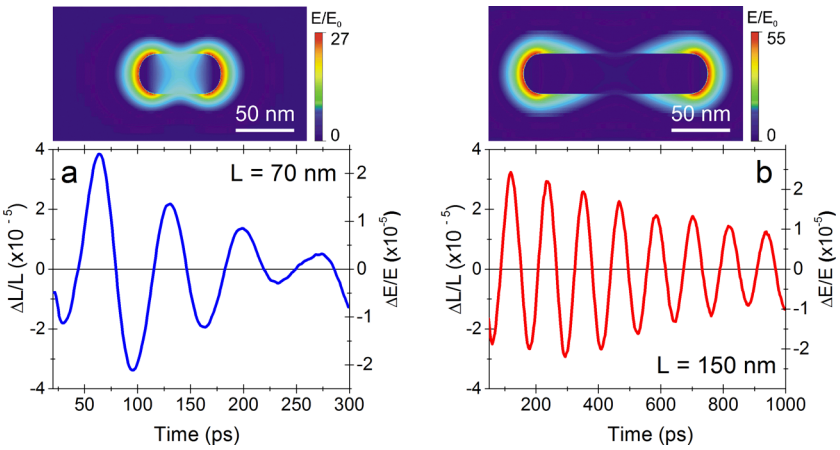

Figure 6. Normalized time-dependent variations $\Delta L/L$ of the NR length and peak energy shift $\Delta E/E$ normalized to the peak of the LSP resonance for the (a) 70 nm and (b) 150 nm sets of gold NRs together with the numerical simulations of the field enhancement at the LSP resonance from FDTD.

DOI: 10.1021/acsnano.5b06904
ACS Nano 2016, 10, 2251−2258

details). The almost instantaneous thermal expansion that follows the optical absorption transfers its energy to both coherent and uncoherent oscillations of the NR. Since many oscillation modes can be excited in the nanoparticle, some of which are predicted to give a negligible differential signal in the pump−probe experiment, a quantitative analysis similar to the one previously performed for nanospheres in a uniform environment[33] is not possible in the present study. However, a simplistic approach based on the use of the linear thermal expansion coefficient for a free-standing Au bar (see Supporting Information for details), together with the experimentally retrieved elongations, provides temperature variations associated with the longitudinal oscillation on the order of 3 K, which is compatible with the values reported above from the two-temperature model.

We believe that the extreme sensitivity of our approach is intrinsic to the method used for the detection of the coherent oscillations which measures, as discussed previously, the first derivative of the absorption spectrum. The ultimate sensitivity of our method is limited only by the signal-to-noise level, which corresponds, in our setup, to a minimum observable energy shift of ≈3 μeV and a minimum observable NR elongation of $\Delta L \approx 0.25$ pm. This also allows us to work with an absorbed energy per NR that is at least 2 orders of magnitude smaller with respect to the values used for recent time-resolved X-ray diffraction experiments.[24,25]

CONCLUSIONS

In this paper, we have quantitatively studied in the time domain the extensional modes in eight different arrays of gold NRs of different lengths, ranging from 70 to 200 nm, by means of ultrafast pump−probe spectroscopy supported by FDTD and eigenvalue analysis simulations. The use of a broadband WLC probe spanning the visible and near-IR energy ranges allowed access to the ultrafast changes of the LSP resonance. We introduce a model that extracts from these tiny optical changes the mechanical deformations of the gold NRs without recurring to the more complex time-resolved X-ray (electron) diffraction spectroscopy. We thus obtain a quantitative evaluation of the longitudinal elongation for the different NRs in a real perturbative regime, namely, for absorbed energies at least 2 orders of magnitude smaller with respect to previous X-ray experiments. In these conditions, we observe a maximum elongation of 3 (5) pm for the 70 (150) nm NRs and a sensitivity on the LSP peak shift of 10^{-5} eV, in good agreement with FDTD simulations. Our work demonstrates a new simple approach for the characterization of mechanical vibrations on a sub-nanometer scale to be applied in all optically controlled nanoscale devices, such as ultrasensitive sensors and resonators.

METHODS

Pump−Probe Spectroscopy. The experimental setup used for the pump−probe studies has been described elsewhere.[34] It is based on a regeneratively amplified Ti:sapphire laser (Coherent, Libra) producing 100 fs, 4 mJ pulses at 1.6 eV photon energy and 1 kHz repetition rate. A portion of this beam was used as the pump pulse. Another fraction of the pulse was focused in a 2 mm thick sapphire plate to generate a broadband single-filament WLC, extending both in the visible and near-IR, that acted as a probe after passing through a delay line. The WLC extended from 1.2 to 1.55 eV and then from 1.65 to 2.8 eV, with a hole at 1.6 eV corresponding to the fundamental laser frequency. The WLC was overlapped with the pump beam on the sample. The transmitted probe light was dispersed on an optical multichannel analyzer equipped with fast electronics, allowing single-shot recording of the probe spectrum at the full 1 kHz repetition rate of the laser. By changing the pump−probe delay, we recorded 2D maps of the differential transmission ($\Delta T/T$) signal as a function of probe wavelength and delay. Our setup achieved, for each probe wavelength, sensitivity down to $\approx 10^{-5}$. Temporal resolution (taken as full width at half-maximum of pump−probe cross-correlation) was ≈180 fs over the entire probe spectrum. The pump fluence used in these experiments was ≈0.1−0.3 mJ/cm^2.

Sample Preparation. Arrays of gold NRs were nanofabricated on a microscope glass slide by a step of electron beam lithography at 100 keV followed by a lift-off of a 20 nm thick layer of gold grown in an electron beam evaporator. The eight different NR arrays differed only by the length, while the height and cross-sectional diameter were kept constant. In particular, the height was ≈20 nm, and the diameter was ≈30 nm. A thin Ge layer (<1 nm) was grown before the deposition of gold in order to reduce its roughness, as previously reported for silver films.[35] The thin Ge layer also improved the adhesion of gold on glass, allowing for an easy lift-off and drastically limiting the damping of the plasmonic resonances as compared with conventional Ti or Cr adhesion layers.[36] A MMA−PMMA resist bilayer was used to obtain an undercut profile that simplifies the lift-off of gold and improves the uniformity of the sample due to the higher sensitivity of the MMA resist to electron exposure.

Numerical Simulations. Full vectorial three-dimensional simulations of the electromagnetic response of the NRs were performed with the FDTD method.[37] The geometry of the NRs, inferred from high-resolution SEM images, was systematically varied in steps of 1 nm while keeping the volume approximately constant, in order to accurately measure the resonance shift in the small perturbation regime. In order to ensure the validity of the results, convergence tests for a mesh size down to about 0.3 nm were performed.

In order to identify the vibrational modes corresponding to the experimental oscillation periods, we performed eigenvalue analysis with COMSOL Multiphysics Solver, using the Structural Mechanics module. This is a commercial software implementing the finite elements method. The simulated cell included a NR with a thin Ge layer onto a glass substrate, which was meshed with triangular elements, whose size was chosen after a convergence analysis. In order to reduce the computational effort, the thickness of simulated glass substrate was taken to be equal to 1.5 μm, as higher thickness did not cause significant differences in the results. With reference to materials physical and mechanical properties, the following values were considered: for gold, Young modulus E_{Au} = 78 GPa,[38] Poisson ratio ν_{Au} = 0.44,[39] mass density ρ_{Au} = 19 320 kg/m^3;[40] for germanium, E_{Ge}= 103 GPa,[41] Poisson ratio ν_{Ge} = 0.26,[42] mass density ρ_{Ge} = 5323 kg/m^3; for glass, E_{glass}= 70 GPa, Poisson ratio ν_{glass} = 0.24, mass density ρ_{glass} = 2600 kg/m^3. The strain energy associated with the considered vibrational mode was estimated by scaling the value obtained from the numerical analysis by a factor $(\varepsilon_{max,exp}/\varepsilon_{max,num})^2$, where $\varepsilon_{max,exp}$ is the maximum experimentally detected strain in the longitudinal direction and $\varepsilon_{max,num}$ is the maximum strain obtained from simulations.

ASSOCIATED CONTENT

Supporting Information

The Supporting Information is available free of charge on the ACS Publications website at DOI: 10.1021/acsnano.5b06904.

Determination of the vibrational modes *via* finite element simulations, and estimation of the lattice heating and thermal elongation with the two-temperature model (PDF)

AUTHOR INFORMATION

Corresponding Authors

*E-mail: gs544@cam.ac.uk.
*E-mail: giulio.cerullo@polimi.it.

DOI: 10.1021/acsnano.5b06904
ACS Nano 2016, 10, 2251−2258

Present Address

[¶](G.S.) Cambridge Graphene Centre, University of Cambridge, 9 JJ Thomson Avenue, Cambridge CB3 0FA, U.K.

Notes

The authors declare no competing financial interest.

ACKNOWLEDGMENTS

We thank M. Finazzi for stimulating discussions. G.C. and N.M.P. are supported by the European Commission under the Graphene Flagship (No. 604391, WP5 "Optoelectronics" and WP10 "Nanocomposites"). N.M.P. is supported by the European Research Council (ERC StG Ideas 2011 BIHSNAM No. 279985 on "Bio-Inspired hierarchical super-nanomaterials", ERC PoC 2013-1 REPLICA2 No. 619448 on "Large-area replication of biological anti-adhesive nanosurfaces", ERC PoC 2013-2 KNOTOUGH No. 632277 on "Super-tough knotted fibers") and by the Provincia Autonoma di Trento ("Graphene Nanocomposites", No. S116/2012-242637 and Reg. Delib. No. 2266). This work was partly supported by the French RENATECH Network.

REFERENCES

(1) Kelly, K. L.; Coronado, E.; Zhao, L. L.; Schatz, G. C. The Optical Properties of Metal Nanoparticles: the Influence of Size, Shape, and Dielectric Environment. *J. Phys. Chem. B* **2003**, *107*, 668−677.

(2) Doria, G.; Conde, J.; Veigas, B.; Giestas, L.; Almeida, C.; Assuncao, M.; Rosa, J.; Baptista, P. V. Noble Metal Nanoparticles for Biosensing Applications. *Sensors* **2012**, *12*, 1657−1687.

(3) Zeng, S.; Yong, K.-T.; Roy, I.; Dinh, X.-Q.; Yu, X.; Luan, F. A Review on Functionalized Gold Nanoparticles for Biosensing Applications. *Plasmonics* **2011**, *6*, 491−506.

(4) Portales, H.; Goubet, N.; Saviot, L.; Adichtchev, S.; Murray, D. B.; Mermet, A.; Duval, E.; Pileni, M.-P. Probing Atomic Ordering and Multiple Twinning in Metal Nanocrystals through their Vibrations. *Proc. Natl. Acad. Sci. U. S. A.* **2008**, *105*, 14784−14789.

(5) Staleva, H.; Hartland, G. V. Vibrational Dynamics of Silver Nanocubes and Nanowires Studied by Single-Particle Transient Absorption Spectroscopy. *Adv. Funct. Mater.* **2008**, *18*, 3809−3817.

(6) Hodak, J. H.; Henglein, A.; Hartland, G. V. Size Dependent Properties of Au Particles: Coherent Excitation and Dephasing of Acoustic Vibrational Modes. *J. Chem. Phys.* **1999**, *111*, 8613.

(7) Voisin, C.; Del Fatti, N.; Christofilos, D.; Vallée, F. Ultrafast Electron Dynamics and Optical Nonlinearities in Metal Nanoparticles. *J. Phys. Chem. B* **2001**, *105*, 2264−2280.

(8) Link, S.; El Sayed, M. A. Spectral Properties and Relaxation Dynamics of Surface Plasmon Electronic Oscillations in Gold and Silver Nanodots and Nanorods. *J. Phys. Chem. B* **1999**, *103*, 8410−8426.

(9) Hodak, J.; Martini, I.; Hartland, G. V. Ultrafast Study of Electron-Phonon Coupling in Colloidal Gold Particles. *Chem. Phys. Lett.* **1998**, *284*, 135−141.

(10) Goubet, N.; Tempra, I.; Yang, J.; Soavi, G.; Polli, D.; Cerullo, G.; Pileni, M. P. Size and Nanocrystallinity Controlled Gold Nanocrystals: Synthesis, Electronic and Mechanical Properties. *Nanoscale* **2015**, *7*, 3237−3246.

(11) Voisin, C.; Del Fatti, N.; Christofilos, D.; Vallée, F. Time-Resolved Investigation of the Vibrational Dynamics of Metal Nanoparticles. *Appl. Surf. Sci.* **2000**, *164*, 131−139.

(12) Zijlstra, P.; Tchebotareva, A. L.; Chon, J. W. M.; Gu, M.; Orrit, M. Acoustic Oscillations and Elastic Moduli of Single Gold Nanorods. *Nano Lett.* **2008**, *8*, 3493−3497.

(13) Ruijgrok, P. V.; Zijlstra, P.; Tchebotareva, A. L.; Orrit, M. Damping of Acoustic Vibrations of Single Gold Nanoparticles Optically Trapped in Water. *Nano Lett.* **2012**, *12*, 1063−1069.

(14) Yu, K.; Zijlstra, P.; Sader, J. E.; Xu, Q.-H.; Orrit, M. Damping of Acoustic Vibrations of Immobilized Single Gold Nanorods in Different Environments. *Nano Lett.* **2013**, *13*, 2710−2716.

(15) Van Dijk, M. A.; Lippitz, M.; Orrit, M. Detection of Acoustic Oscillations of Single Gold Nanospheres by Time-Resolved Interferometry. *Phys. Rev. Lett.* **2005**, *95*, 267406.

(16) Li, M.; Tang, H. X.; Roukes, M. L. Ultra-Sensitive NEMS-Based Cantilevers for Sensing, Scanned Probe and Very High Frequency Applications. *Nat. Nanotechnol.* **2007**, *2*, 114−120.

(17) Verbridge, S. S.; Bellan, L. M.; Parpia, J. M.; Craighead, H. G. Optically Driven Resonance on Nanoscale Flexural Oscillators in Liquid. *Nano Lett.* **2006**, *6*, 2109−2114.

(18) Naik, A. K.; Hanay, M. S.; Hiebert, W. K.; Feng, X. L.; Roukes, M. L. Towards Single-Molecule Nanomechanical Mass Spectrometry. *Nat. Nanotechnol.* **2009**, *4*, 445−450.

(19) Anderson, A.; Deryckx, K. S.; Xu, X. G.; Steinmeyer, G.; Raschke, M. B. Few-Femtosecond Plasmon Dephasing of a Single Metallic Nanostructure from Optical Response Function Reconstruction by Interferometric Frequency Resolved Optical Gating. *Nano Lett.* **2010**, *10*, 2519−2524.

(20) Sun, C.-K.; Vallée, F.; Acioli, L. H.; Ippen, E. P.; Fujimoto, J. G. Femtosecond-Tunable Measurement of Electron Thermalization in Gold. *Phys. Rev. B: Condens. Matter Mater. Phys.* **1994**, *50*, 15337.

(21) Della Valle, G.; Conforti, M.; Longhi, S.; Cerullo, G.; Brida, D. Real-Time Optical Mapping of the Dynamics of Nonthermal Electrons in Thin Gold Films. *Phys. Rev. B: Condens. Matter Mater. Phys.* **2012**, *86*, 155139.

(22) Hartland, G. V. Optical Studies of Dynamics in Noble Metal Nanostructures. *Chem. Rev.* **2011**, *111*, 3858−3887.

(23) Hu, M.; Wang, X.; Hartland, G. V.; Mulvaney, P.; Juste, J. P.; Sader, J. E. Vibrational Response of Nanorods to Ultrafast Laser Induced Heating: Theoretical and Experimental Analysis. *J. Am. Chem. Soc.* **2003**, *125*, 14925−14933.

(24) Clark, J. N.; Beitra, L.; Xiong, A.; Higginbotham, A.; Fritz, D. M.; Lemke, H. T.; Zhu, D.; Chollet, M.; Williams, G. J.; Messerschmidt, M.; Abbey, B.; Harder, R. J.; Korsunsky, A. M.; Wark, J. S.; Robinson, I. K. Ultrafast Three-Dimensional Imaging of Lattice Dynamics in Individual Gold Nanocrystals. *Science* **2013**, *341*, 56−59.

(25) Szilagyi, E.; Wittenberg, J. S.; Miller, T. A.; Lutker, K.; Quirin, F.; Lemke, H.; Zhu, D.; Chollet, M.; Robinson, J.; Wen, H.; Sokolowski-Tinten, K.; Lindenberg, A. M. Visualization of Nanocrystal Breathing Modes at Extreme Strains. *Nat. Commun.* **2015**, *6*, 6577.

(26) Ruan, C.-Y.; Murooka, Y.; Raman, R. K.; Murdick, R. A. Dynamics of Size-Selected Gold Nanoparticles Studied by Ultrafast Electron Nanocrystallography. *Nano Lett.* **2007**, *7*, 1290−1296.

(27) Gans, R. Über die Form Ultramikroskopischer Silberteilchen. *Ann. Phys.* **1915**, *47*, 270−284.

(28) Link, S.; Mohamed, M. B.; El-Sayed, M. A. Simulation of the Optical Absorption Spectra of Gold Nanorods as a Function of Their Aspect Ratio and the Effect of the Medium Dielectric Constant. *J. Phys. Chem. B* **1999**, *103*, 3073−3077.

(29) Johnson, P. B.; Christy, R. W. Optical Constants of Noble Metals. *Phys. Rev. B* **1972**, *6*, 4370−4379.

(30) Major, T. A.; Crut, A.; Gao, B.; Lo, S. S.; Del Fatti, N.; Vallée, F.; Hartland, G. V. Damping of the Acoustic Vibrations of a Suspended Gold Nanowire in Air and Water Environments. *Phys. Chem. Chem. Phys.* **2013**, *15*, 4169.

(31) Frangi, A.; Cremonesi, M.; Jaakkola, A.; Pensala, T. Analysis of Anchor and Interface Losses in Piezoelectric MEMS Resonators. *Sens. Actuators, A* **2013**, *190*, 127−135.

(32) Wang, Z.; Tian, B.; Van Thourhout, D. Design of a Novel Micro-Laser Formed by Monolithic Integration of a III-V Pillar With a Silicon Photonic Crystal Cavity. *J. Lightwave Technol.* **2013**, *31* (9), 1475−1481.

(33) Hartland, G. V. Coherent Vibrational Motion in Metal Nanoparticles: Determination of the Vibrational Amplitude and Excitation Mechanism. *J. Chem. Phys.* **2002**, *116*, 8048−8055.

DOI: 10.1021/acsnano.5b06904
ACS Nano 2016, 10, 2251−2258

(34) Polli, D.; Luer, L.; Cerullo, G. High-Time-Resolution Pump-Probe System with Broadband Detection for the Study of Time-Domain Vibrational Dynamics. *Rev. Sci. Instrum.* **2007**, *78*, 103108.
(35) Logeeswaran, V. J.; Kobayashi, N. P.; Islam, M. S.; Wu, W.; Chaturvedi, P.; Fang, N. X.; Wang, S. Y.; Williams, R. S. Ultrasmooth Silver Thin Films Deposited with a Germanium Nucleation Layer. *Nano Lett.* **2009**, *9*, 178−182.
(36) Aouani, H.; Wenger, J.; Gérard, D.; Rigneault, H.; Devaux, E.; Ebbesen, T. W.; Mahdavi, F.; Xu, T.; Blair, S. Crucial Role of the Adesion Layer on the Plasmonic Fluorescence Enhancement. *ACS Nano* **2009**, *3*, 2043−2048.
(37) *FDTD Solutions*; Lumerical Inc., Canada.
(38) Wu, B.; Heidelberg, A.; Boland, J. J. Mechanical Properties of Ultrahigh-Strength Gold Nanowires. *Nat. Mater.* **2005**, *4*, 525−529.
(39) Weng, C.-J. Integrated Process Feasibility of Hard-Mask for Tight Pitch Interconnects Fabrication. *MEMS and Nanotechnology*; Springer, 2011.
(40) Callister, W. D. *Materials Science and Engineering*; John Wiley & Sons, Inc., 2007.
(41) Smith, D. A.; Holmberg, V. C.; Lee, D. C.; Korgel, B. A. Young's Modulus and Size-Dependent Mechanical Quality Factor of Nano-electromechanical Germanium Nanowire Resonators. *J. Phys. Chem. C* **2008**, *112*, 10725−10729.
(42) Wortman, J. J.; Evans, R. A. Young's Modulus, Shear Modulus, and Poisson's Ratio in Silicon and Germanium. *J. Appl. Phys.* **1965**, *36*, 153−156.

DOI: 10.1021/acsnano.5b06904
ACS Nano 2016, 10, 2251−2258

Supporting Information for

Ultra-Sensitive Characterization of Mechanical Oscillations and Plasmon Energy Shift in Gold Nanorods

Giancarlo Soavi[1]†, Iacopo Tempra[1], Maria F. Pantano[2], Andrea Cattoni[3], Stéphane Collin[3], Paolo Biagioni[1], Nicola M. Pugno[2, 4,5], Giulio Cerullo[1,6]**

1. Department of Physics, Politecnico di Milano, P.zza L. Da Vinci 32, 20133, Milano, Italy
2. Laboratory of Bio-inspired & Graphene Nanomechanics, Department of Civil, Environmental and Mechanical Engineering, Università di Trento, via Mesiano 77, 38123 Trento, Italy
3. Laboratoire de Photonique et de Nanostructures, CNRS, Université Paris-Saclay, route de Nozay, F-91460 Marcoussis, France
4. Center for Materials and Microsystems, Fondazione Bruno Kessler, Via Sommarive 18, 38123 Povo (TN), Italy
5. School of Engineering and Materials Science, Queen Mary University of London, Mile End Road, London E1 4NS, U.K.
6. IFN-CNR, P.zza L. Da Vinci 32, 20133, Milano, Italy

S1. Determination of the vibrational modes via Finite Element Simulations

The FE simulations based on our specific sample geometry retrieved five possible mechanical oscillations with a period similar to the one observed experimentally. From this, we selected only two modes (shown in figure 3e of the manuscript) based on a direct comparison of the period VS nanorod (NR) length dependence (see figure S1). The choice of these modes was possible thanks to the experimental availability of a large range of NR aspect ratios. Given a single NR geometry, the choice among different possible vibrational modes simply based on the values for the oscillation period obtained from FE simulations could indeed be misleading. The modes that contribute to the transient optical signal are those that produce the largest change in volume/aspect ratio, which naturally translates into the strongest effect on the extinction coefficient. Although this was not the criterion to select the vibrational modes presented in this work, we could *a posteriori* observe that the selected modes were also the ones that affected the most the NR aspect ratio (modes 4 and 5).

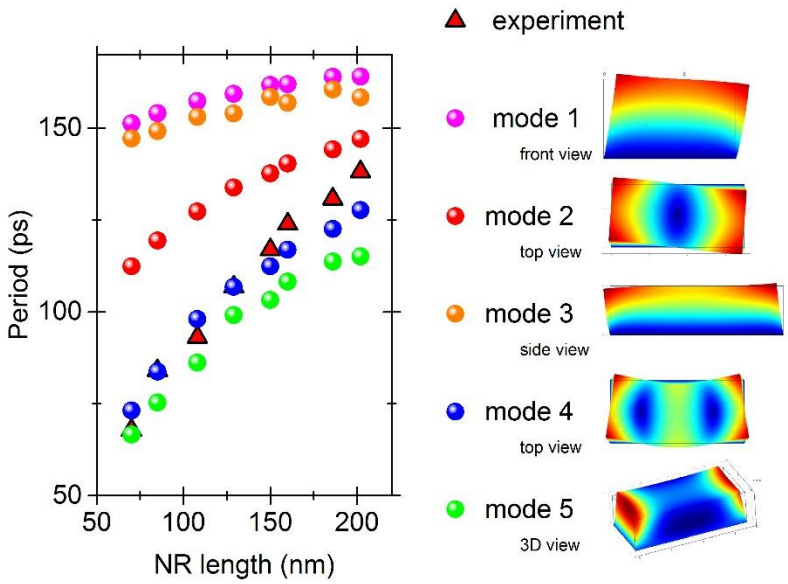

Figure S1. Circles: calculated oscillation period as a function of NR length for 5 vibrational modes obtained by FE simulations. Triangles: experimentally measured periods.

S2. Two-temperature model and thermal elongation

We can calculate the lattice temperature increase after pulsed excitation with the two-temperature model

$$C_{\mathrm{e}}(T_{\mathrm{e}})\frac{dT_{\mathrm{e}}}{dt} = -g(T_{\mathrm{e}} - T_{\mathrm{L}}) + \frac{E_0}{\sqrt{\pi}\sigma_{\mathrm{L}}} e^{-t^2/\sigma_{\mathrm{L}}^2}$$

$$C_{\mathrm{L}}\frac{dT_{\mathrm{L}}}{dt} = g(T_{\mathrm{e}} - T_{\mathrm{L}}) - \frac{T_{\mathrm{L}} - 298\ \mathrm{K}}{\tau_{\mathrm{S}}}$$

where T_{e} and T_{L} are the electron and lattice temperature respectively, $C_{\mathrm{e}}(T_{\mathrm{e}}) = \xi T_{\mathrm{e}}$ ($\xi = 68\ \mathrm{JK^{-2}m^{-3}}$) is the temperature dependent electron heat capacity, C_{L} ($C_{\mathrm{L}} = 2.5\ 10^6\ \mathrm{JK^{-1}m^{-3}}$) is the lattice heat capacity, g ($g = 2.2\ \mathrm{WK^{-1}m^{-3}}$) is the electron phonon coupling constant, E_0 is the density of energy absorbed by the sample, σ_{L} is the temporal pulse-width and τ_{S} is the time-scale for energy transfer to the ambient. Our temporal resolution is $\sigma_{\mathrm{L}} = 0.18\ \mathrm{ps}$ and for simplicity we assume $\tau_{\mathrm{S}} \approx 400\ \mathrm{ps}$. We note that τ_{S} only affects the relaxation (decrease) of T_{L} on a long time-scale and not its maximum value (that is reached after ≈ 5 - 10 ps), thus we do not need any further study to evaluate this parameter. Given the fluencies employed during the experiments (between 100 and 300 μJ/cm^2) and the simulated absorption cross sections of the nanoparticles (of the order of 10^3 to 10^4 nm^2 for different NR lengths), application of the two-temperature model predicts an increase in the lattice temperature roughly between 5 and 50 K.

The linear thermal expansion can be simply calculated as $\Delta L = \alpha \Delta T_{\mathrm{L}} L_0$, where $\alpha \approx 14.3\ 10^{-6}\ \mathrm{K^{-1}}$ is the linear thermal expansion coefficient of gold. If we calculate the increase in lattice temperature responsible for the experimentally observed elongation associated

with the observed longitudinal acoustic mode we obtain $\Delta T_{\mathrm{L}}^{\mathrm{exp}} = \frac{\Delta L}{\alpha L_0} \approx 3$ K for both the 70 and 150 nm NR, which is compatible with the values reported above from the two-temperature model.